

Multilevel atomic Ramsey interferometry for precise parameter estimations

X N Feng(冯夏宁) and L F Wei(韦联福)

Citation: Chin. Phys. B, 2021, 30 (**12**): 120601. DOI: 10.1088/1674-1056/ac0527
Journal homepage: http://cpb.iphy.ac.cn; http://iopscience.iop.org/cpb

What follows is a list of articles you may be interested in

A 532 nm molecular iodine optical frequency standard based on modulation transfer spectroscopy

Feihu Cheng(程飞虎), Ning Jin(金宁), Fenglei Zhang(张风雷), Hui Li(李慧), Yuanbo Du(杜远博), Jie Zhang(张洁), Ke Deng(邓科), and Zehuang Lu(陆泽晃)
Chin. Phys. B, 2021, 30 (**5**): 050603. DOI: 10.1088/1674-1056/abd754

An Yb-fiber frequency comb phase-locked to microwave standard and optical reference

Hui-Bo Wang(汪会波), Hai-Nian Han(韩海年), Zi-Yue Zhang(张子越), Xiao-Dong Shao(邵晓东), Jiang-Feng Zhu(朱江峰), Zhi-Yi Wei(魏志义)
Chin. Phys. B, 2020, 29 (**3**): 030601. DOI: 10.1088/1674-1056/ab696d

Phase sensitivity of two nonlinear interferometers with inputting entangled coherent states

Chao-Ping Wei(魏朝平), Xiao-Yu Hu(胡小玉), Ya-Fei Yu(於亚飞), Zhi-Ming Zhang(张智明)
Chin. Phys. B, 2016, 25 (**4**): 040601. DOI: 10.1088/1674-1056/25/4/040601

Enhancing the precision of phase estimation by weak measurement and quantum measurement reversal

He Zhi, Yao Chun-Mei
Chin. Phys. B, 2014, 23 (**11**): 110601. DOI: 10.1088/1674-1056/23/11/110601

Quantum metrology

Xiang Guo-Yong, Guo Guang-Can
Chin. Phys. B, 2013, 22 (**11**): 110601. DOI: 10.1088/1674-1056/22/11/110601

Multilevel atomic Ramsey interferometry for precise parameter estimations*

X N Feng(冯夏宁)[1,2,†] and L F Wei(韦联福)[2,‡]

[1] Guangdong Provincial Key Laboratory of Quantum Metrology and Sensing & School of Physics and Astronomy, Sun Yat-Sen University (Zhuhai Campus), Zhuhai 519082, China

[2] Information Quantum Technology Laboratory, School of Information Science and Technology, Southwest Jiaotong University, Chengdu 610031, China

(Received 26 January 2021; revised manuscript received 24 April 2021; accepted manuscript online 26 May 2021)

Multi-path (or multi-mode) entanglement has been proved to be a useful resource for sub-shot-noise sensitivity of phase estimation, which has aroused much research interest in quantum metrology recently. Various schemes of multi-path interferometers based on optical systems have been put forward. Here, we study a multi-state interferometer with multi-level atoms by projective measurements. Specifically, we investigate its ultimate sensitivity described by quantum Fisher information theory and find that the Cramer–Rao bound can be achieved. In particular, we investigate a specific scheme to improve the sensitivity of magnetometery with a three-state interferometry delivered by a single nitrogen-vacancy (NV) center of diamond with tailor pulses. The impacts of imperfections of the atomic beam-splitter, described by the three-level quantum Fourier transform, on the sensitivity of phase estimation is also discussed.

Keywords: quantum metrology, multi-path interferometers, quantum measurement

PACS: 06.20.–f, 06.20.Dk, 03.75.Dg **DOI:** 10.1088/1674-1056/ac0527

1. Introduction

It is well-known that interferometers (IFRs) are particularly important state-of-the-art setups in present-day precise measurements,[1] e.g., for the atomic clocks, sensitive magnetometery, and the quantum manipulations of qubits. Indeed, beginning with the original Ramsey IFR by using a two-level atom[2] or its formally equivalent Mach–Zehnder IFR with two optical paths,[3–5] various generalized versions of IFRs have been developed for many metrologic applications.[6–8] For example, the squeezed light IFRs for gravitational wave detections,[9–11] the matter wave IFRs with cold atoms (with the shorter de Broglie wavelengths) for the precise measurements of gravity and fine structure constants,[12–15] and also the Sagnac IFRs for rotation measurements,[16] etc.

Practically, any measurement is a physical process and the measured system is always influenced by its environments. As a consequence, the available accuracy of the measured quantities is limited by certain fundamental laws. For example, due to the shot noise, the optimal accuracy of the phase estimation by usual two-level atomic Ramsey-type IFRs (after N trials) is $\Delta\phi \geq 1/\sqrt{N}$. This is the standard quantum limit (SQL), which cannot be beaten unless certain nonclassical resources[17–19] (such as the squeezing states[20–23] and entangled atomic NOON states[24,25]) are utilized.

Given that the quantum many-body entanglements are very fragile and also hard to be prepared, an alternative way for improving the interferometer sensitivity by using the multi-path interferometry have attracted much attention in recent years.[25–31] Physically, the resolution of the interferometric signals and thus the sensitivity of the relevant IFRs can be improved by increasing the number of interference paths. In this kind of multi-mode interferometers, the realization of the beam-splitter (BS) for the separation and recombination of the multi-mode evolutions is the key operation, which can be theoretically described by a $N \times N$ quantum Fourier transformation (QFT) for N-mode interferometers.[26] For instance, the passive linear optical devices with uncorrelated single-photon inputs[26–30] for optical interferometers, the Kapitza–Dirac pulse[15] for implementing the sub-shot noise limit of atomic interferometers.[32] It is shown theoretically that, the sensitivity of phase estimation can be enhanced to beat the shot-noise limit (SNL) with respective to the number of interference paths.[26] The imperfection of the multi-path optical interferometers, due to photon losses, is also investigated.[28] Specifically, the recent experiment,[33] demonstrated by a five-state interferometer, showed the 1.75 times resolution higher than that with the usual two-state one.

Inspired by the above demonstrations, in this paper we propose a multi-state atomic interferometry with a multi-level atom to implement the precise estimation of an unknown relative phase θ, and then specially apply it to implement the sensitive magnetometery with a nitrogen-vacancy (NV) color center. Differing from the previous multi-state IFRs with the simultaneous multi-state measurements (see, e.g., Refs. [26,33]), here the measurement of a single atomic state

*Project supported by the National Natural Science Foundation of China (Grant No. 11974290).

†Corresponding author. E-mail: fengxianing@163.com

‡Corresponding author. E-mail: lfwei@swjtu.edu.cn

© 2021 Chinese Physical Society and IOP Publishing Ltd

is enough for certain phases. We find that the optimal sensitivity of phase estimation is reduced by a factor $1/\sqrt{F_Q}$, where $F_Q = (M^2-1)/3$ denotes the quantum Fisher information (QFI) of the output atomic states with M being the numbers of atomic energy levels. Furthermore, the feasibility of the compact multilevel atomic IFRs proposed here is demonstrated with a single three-level NV center in diamond driven by proper pulses. The effects of unperfect implementations of the QFT on the sensitivity of the phase estimation is also analyzed.

2. M-level atomic Ramsey IFRs to estimate unknown relative phases

The configuration of the proposed IFR is shown in Fig. 1, which reduces to the original Ramsey one if (i) the M-level atom is replaced by a two-level one and (ii) a pair of M-dimensional QFTs are simplified to a pair of Hadamard gates. For the formal simplicity, we first assume that the splittings between two nearest-neighbor atomic levels are equivalent. As a consequence, the M-level atom can be described by the Hamiltonian $H_a = \sum_{k=1}^{M} \hbar\omega_k |k\rangle\langle k|$, $\omega_k = k\omega_1$, with ω_1 being the transition frequency between the two nearest-neighbor levels. After the first M-dimensional QFT, $U_{\rm QFT}^{(M)} = \left(A_{k,l}\right)$, $A_{kl} = \exp[2{\rm i}\pi(k-1)(l-1)/M]/\sqrt{M}, k,l = 1,\ldots,M$, the atom initially in state $|1\rangle$ is evolved into the supposition state $|\psi_{\rm in}\rangle = \sum_{k=1}^{M}|k\rangle/\sqrt{M}$. Next, the atom undergoes a free evolution for the duration t, described by a diagonal matrix $V(\theta) = \exp({\rm i}k\theta)\delta_{kj}$, and its state becomes $|\psi(\theta)\rangle = \sum_{k=1}^{M} {\rm e}^{{\rm i}\phi_k}|k\rangle/\sqrt{M} = \sum_{k=1}^{M} {\rm e}^{{\rm i}k\theta}|k\rangle/\sqrt{M}$, with $\theta = \omega_1 t$ being the phase desired to be estimated. Then, another M-dimensional inverse QFT is applied to evolve the atom into the state $|\psi_{\rm out}(\theta)\rangle = U_{\rm QFT}^{(M)\dagger}|\psi(\theta)\rangle$. This means that the operational procedure for the phase estimation demonstrated above can be expressed by the evolution operator $T(\theta) = U_{\rm QFT}^{(M)\dagger} V(\theta) U_{\rm QFT}^{(M)}$, which evolves the input atomic state $|1\rangle$ to the output one: $|\psi_{\rm out}(\theta)\rangle = T(\theta)|1\rangle$. The matrix elements of the operator $T(\theta)$ read

$$T(\theta)_{kl} = \frac{1}{M}\sum_{j=1}^{M} \exp\left\{{\rm i}\left[j\theta + \frac{2\pi}{M}(j-1)(k-l)\right]\right\}, \quad (1)$$

from which the output atomic state can be specifically written as

$$|\psi_{\rm out}(\theta)\rangle = \frac{1}{M}\sum_{k=1}^{M}\exp({\rm i}k\theta)\sum_{l=1}^{M} \times \exp\left[\frac{2{\rm i}\pi}{M}(l-1)(k-1)\right]|l\rangle. \quad (2)$$

Finally, we perform a projective measurement $\hat{P}_k = |k\rangle\langle k|$ or a POVM $\{|k\rangle\langle k|\}$ to collapse the atomic superposition state into the state $|k\rangle$ with the probability

$$P_k(\theta) = \langle\psi_{\rm out}(\theta)|\hat{P}_k|\psi_{\rm out}(\theta)\rangle = \frac{1-\cos(M\theta)}{M^2\left(1-\cos\left(\theta-\frac{2k\pi}{M}\right)\right)}. \quad (3)$$

With such an experimental interference distribution, the information of the desired relative phase θ can be extracted. Equation (3) shows that the population of the state $|k\neq 1\rangle$ is just a phase shift $2k\pi/M$ compared with state $|1\rangle$.

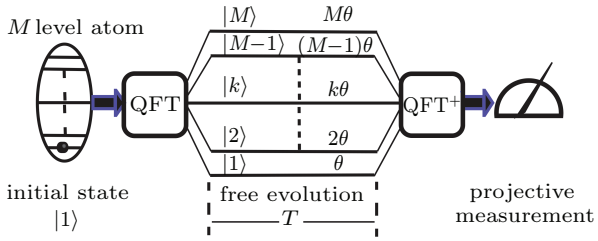


Fig. 1. The schematic of an M-level atomic IFR, implemented by two QFTs in a projective measurement of the atom, for estimating the relative phase θ acquired by a free evolution.

We now discuss what is the uncertainty $\Delta\theta_M$ of the measured phase θ by running the above IFR after N trials. This can be determined by using the well-known error-propagation formula and the Cramer–Rao inequality.[34] For example, for a single projective measurement on the state $|1\rangle$, we have

$$\Delta\theta_M = \frac{1}{\sqrt{N}}\frac{\Delta P_1(\theta)}{\left|\frac{{\rm d}P_1(\theta)}{{\rm d}\theta}\right|} \geq \frac{1}{\sqrt{NF_Q(|\psi_{\rm out}(\theta)\rangle)}} = \Delta\theta_{\rm min}^{(M)}, \quad (4)$$

with $\Delta P_1(\theta) = \sqrt{\langle\hat{P}_1^2(\theta)\rangle - \langle\hat{P}_1(\theta)\rangle^2}$ being the uncertainty and

$$F_Q(|\psi_{\rm out}(\theta)\rangle) = \frac{M^2-1}{3} \quad (5)$$

the θ-independent QFI of the state $|\psi_{\rm out}\rangle$. Equation (5) indicates clearly that the SQL in the original Ramsey IFRs can be really enhanced by running the M-level atomic IFRs for $M \geq 3$.

The question is if the optimal sensitivity $\Delta\theta_{\rm min}^{M}$ of the phase measurements with the above IFRs is reachable. From Eq. (3), we have

$$\frac{{\rm d}P_1(\theta)}{{\rm d}\theta} = \frac{M\sin(M\theta)(1-\cos\theta) - [1-\cos(M\theta)]\sin\theta}{M^2(1-\cos\theta)^2}, \quad (6)$$

$$(\Delta P_1(\theta))^2 = \frac{1-\cos(M\theta)}{M^4(1-\cos\theta)^2} \times \left[M^2(1-\cos\theta)+\cos(M\theta)-1\right]. \quad (7)$$

Furthermore, from Eqs. (6) and (7) we have

$$\frac{\Delta P_1(\theta)}{\left|\frac{\partial P_1(\theta)}{\partial\theta}\right|} = \frac{|\sin(\frac{\theta}{2})|\sqrt{M^2\sin^2(\frac{\theta}{2}) - \sin^2(\frac{M\theta}{2})}}{|M\cos(\frac{M\theta}{2})\sin(\frac{\theta}{2}) - \sin(\frac{M\theta}{2})\cos(\frac{\theta}{2})|}, \quad (8)$$

which is related to both the number M of the atomic levels and the θ with a period of 2π. This implies that, by properly

selecting the number M of the atomic levels the optimal sensitivity $\Delta\theta_{\min}^{M}$ could be achievable for certain estimated phases. More clearly, Fig. 2 shows the attainability of such an optimal sensitivity, i.e., $\Delta_A^{(M)} = \Delta\theta_{\min}^{(M)}/\Delta\theta_M$, versus the number M of the atomic levels and the estimated phase θ within a minimal period 2π. It is seen that:

(i) If the estimated phase $\theta \ll 1$, the uncertainty $\Delta\theta_M \to \sqrt{3}/(\sqrt{N}\sqrt{M^2-1})$. This means that the relevant Cramer–Rao bound can always be achieved and the M-dependent minimal uncertainty $\Delta\theta_{\min}^{(M)}$ defined in Eq. (5) is realized, which beats the original two-level SQL for $M \geq 3$. Certainly, for the phases estimated near $2k\pi, (k = 0, 1, 2\ldots)$, the greater number M of the atomic levels used in the IFRs implies the lower bounds which can be achievable.

(ii) The effective range of the phase θ that can be optimally measured, i.e., approaching the Cramer–Rao bound,[34] decreases with the number M of the atmoic levels. This effective range can be estimated as $[(2k-3)\pi/M, (2k-1)\pi/M]$ for each single projective measurement $\hat{P}_k = |k\rangle\langle k|$ as shown in Fig. 3. Specifically, for the original Ramsey IFRs with $M = 2$ any phase θ with $\theta \in [0, 2\pi]$ can be estimated with the accuracy arriving at Cramer–Rao bound, i.e., $\Delta_A^{(2)} = 1$.

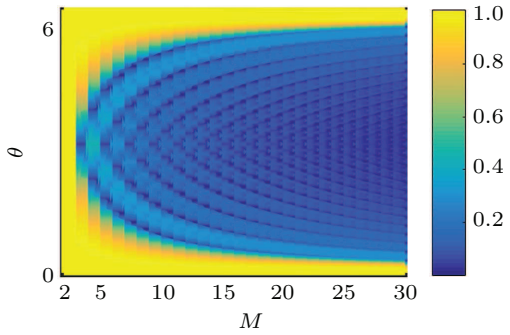


Fig. 2. Attainability $\Delta_A^{(M)} = \Delta\theta_{\min}^{(M)}/\Delta\theta_M$ (of Eq. (4)) of the sensitivity of the phase measurements versus the number M of the atomic levels and the estimated phase θ by a single projective measurement of ground state $|1\rangle$.

The above observations indicate that, although the M-level atomic IFRs proposed here could be utilized to improve the sensitivity of the phase estimation, the region (within a 2π period) optimal is limited for a single projective measurement on a certain state. Fortunately, most of the phases estimated with the practical IFR applications, e.g., the sensitivity magnetometery, gravitater and fine-structure constants, are sufficiently small, and thus the present IFRs should be robustness.

In fact, the tradeoff between the sensitivity and effective range can be overcome by performing a POVM $\{|k\rangle\langle k|\}$ instead of a single projective measurement. This is because every projective measurement covers a separate effective regime, the sum in measurements just covers the whole regime of $[0, 2\pi]$ as shown in Fig. 3. Actually, this can be viewed from the perspective of Fisher information with respective to the POVM of projective measurement. This is verified numerically in Fig. 4.

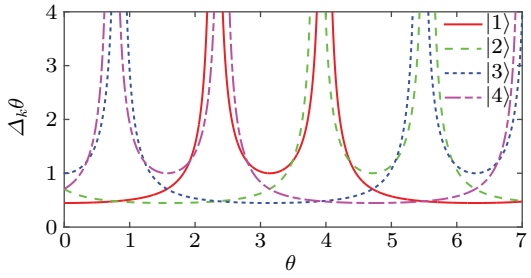


Fig. 3. The phase estimation sensitivity $\Delta_k\theta = \Delta P_k(\theta)/|\partial_\theta P_k(\theta)|$ of different projective measurements $|k\rangle\langle k|$ as a function of phase θ, for the number of levels $M = 4$ as an example. Each single projective measurement has its own optimal parameter regime that can approach the ultimate bound of QFI.

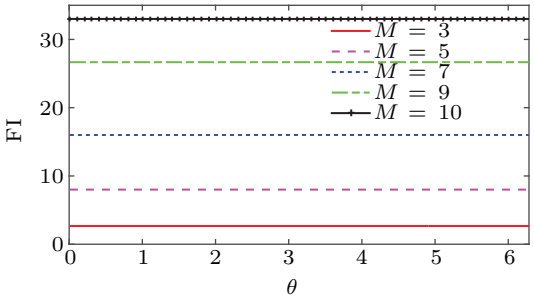


Fig. 4. The Fisher information corresponding to the POVM measurement $\{|k\rangle\langle k|\}$, defined as $F(\theta) = \sum_{k=1}^{m} |\partial_\theta P_k(\theta)|^2/P_k(\theta)$, as a function of phase θ, for various number of levels, which just achieve the QFI $F_Q(|\psi_{\text{out}}(\theta)\rangle)$ of Eq. (5).

It is worth emphasizing that the above assumption of equivalent energy splittings to simplify the presentation of our generic proposal is practically unnecessary. In fact, for the multilevel atoms with inequivalent energy splittings, certain additional quantum operations, typically such as the spin-echo-like ones, can be added to refocus the unwanted additional dynamical phases. This implies that the proposed IFRs should still work, even for the generic multilevel atoms.

3. Improving the sensitivity of the magnetometery with the IFRs using three-level NV centers in diamond

Single NV centers in diamond are perfect quantum objects to implement quantum coherent manipulations, as they possess significantly long coherence times and can be operated at room temperature. In fact, a series of experiments have been recently demonstrated to implement the IFRs using single NV centers with two Zeeman levels for magnetic sensors at nanoscale space resolutions, see, e.g., Refs. [35,36] and references therein. Typically, a 3 nT magnetic field has been detected at the sensitivity of 0.5 μT·Hz$^{-1/2}$ for a diamond nanocrystal with a diameter of 30 nm.[37] However, the further improvements of the sensitivity with the standard IFRs would be principally limited by the SQL bound.

By just generalizing the IFRs with two-level NV centers to those with three-level ones, we now specifically demonstrate that the original two-level SQL can be enhanced. Without loss of generality, we consider the simplest V-type three-level configuration of the NV center shown in Fig. 5, wherein $D_{\rm gs}-\omega_{21}=\omega_{31}-D_{\rm gs}$ and $\omega_{jk}=\omega_j-\omega_k, j>k$. Here, $D_{\rm gs}$ is the ground triplet-state zero-field splitting, i.e., the Zeeman splitting of $S=1$, which is proportional to the projection of the applied magnetic field along the NV symmetry axis.

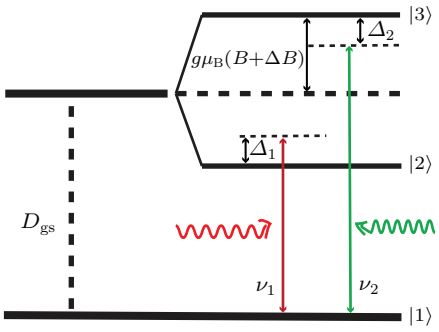


Fig. 5. The lower three Zeeman levels and their transition relations of an NV center in diamond. Here, g denotes g-factor, $\mu_{\rm B}$ is the Bohr magneton, ν_i with $i=1,2$ is the frequency of the allowed transition, and B is supposed as a given applied magnetic field to obtain the desired frequencies ω_2 and ω_3, while ΔB is the weak magnetic field expected to be measured.

As mentioned above, the key of our phase estimation algorithm with the proposed M-level IFRs is to implement the relevant QFT operations. For the present three-level system, the QFT reads[38]

$$U_{\rm QFT}^{(3)}={\rm i}U_DU_3U_2U_1, \tag{9}$$

with

$$U_1=\begin{pmatrix}-1 & 0 & 0\\ 0 & -\frac{1}{\sqrt{2}} & -\frac{{\rm e}^{{\rm i}2\pi/3}}{\sqrt{2}}\\ 0 & -\frac{{\rm e}^{-{\rm i}2\pi/3}}{\sqrt{2}} & \frac{1}{\sqrt{2}}\end{pmatrix},$$

$$U_2=\begin{pmatrix}-\sqrt{\frac{2}{3}} & \frac{{\rm i}\,{\rm e}^{{\rm i}\pi/6}}{\sqrt{3}} & 0\\ \frac{{\rm i}\,{\rm e}^{-{\rm i}\pi/6}}{\sqrt{3}} & -\sqrt{\frac{2}{3}} & 0\\ 0 & 0 & 1\end{pmatrix},$$

$$U_3=\begin{pmatrix}\frac{1}{\sqrt{2}} & 0 & \frac{{\rm i}\,{\rm e}^{-{\rm i}2\pi/3}}{\sqrt{2}}\\ 0 & 1 & \\ \frac{{\rm i}\,{\rm e}^{{\rm i}2\pi/3}}{\sqrt{2}} & 0 & \frac{1}{\sqrt{2}}\end{pmatrix},$$

$$U_D=\begin{pmatrix}{\rm e}^{-{\rm i}\pi/2} & 0 & 0\\ 0 & {\rm e}^{{\rm i}\pi/6} & 0\\ 0 & 0 & {\rm e}^{{\rm i}\pi/3}\end{pmatrix}.$$

The evolutions $U_{k=1,2,3,D}$ to implement the required QFT can be successively achieved by applying the relevant microwave pluses designed accordingly.

First, to realize the U_1-evolution using the transition $|1\rangle\leftrightarrow|2\rangle$, which is practically dipole forbidden, we apply two microwave pulses with the frequencies ν_1 and ν_2, respectively. These pulses drive the system by the following Hamiltonian:

$$\begin{aligned}H(t)=&\sum_{j=1}^{3}\omega_j|j\rangle\langle j|+\{\Omega_1^*\,{\rm e}^{{\rm i}\nu_1 t}|1\rangle\langle 2|\\&+\Omega_2^*\,{\rm e}^{{\rm i}\nu_2 t}|1\rangle\langle 3|+{\rm H.c.}\},\end{aligned} \tag{10}$$

under the usual rotating-wave approximation. Here, Ω_1 and Ω_2 are the relevant Rabi frequencies. Furthermore, under the large detuning limit the above Hamiltonian becomes

$$\begin{aligned}\widetilde{H}_1=&\frac{-3}{2}\left(\frac{|\Omega_1|^2}{\Delta_1}+\frac{|\Omega_2|^2}{\Delta_2}\right)|1\rangle\langle 1|\\&+\left(\frac{|\Omega_1|^2}{\Delta_1}-\frac{|\Omega_2|^2}{\Delta_2|^2}\right)(|2\rangle\langle 2|-|3\rangle\langle 3|)\\&+\frac{\Omega_1\Omega_2^*}{2}\left(\left(\frac{1}{\Delta_1}+\frac{1}{\Delta_2}\right)|2\rangle\langle 3|+{\rm H.c.}\right).\end{aligned} \tag{11}$$

By setting $\Delta=\Delta_1=\Delta_2$, $\Delta_1=\omega_{21}-\nu_1$ and $\Delta_2=\omega_{31}-\nu_2$, This Hamiltonian delivers the evolution

$$\widetilde{U}_1={\rm i}\exp\left[-3{\rm i}(|\Omega_1|^2+|\Omega_2|^2)\frac{t_1}{2\Delta}-\frac{{\rm i}\pi}{2}\right]|1\rangle\langle 1|U_1, \tag{12}$$

where $\Delta_0=(|\Omega_2|^2-|\Omega_1|^2)/(2\Delta)$, $\Omega_0=\Omega_1^*\Omega_2/\Delta$, $\Omega=\sqrt{\Delta_0^2+\Omega_0^2}$, and $\Omega t_1=3\pi/2$, $\Delta_0=|\Omega_0|$, $\Omega_0=|\Omega_0|\,{\rm e}^{-2{\rm i}\pi/3}$. Turning back to the original basis $\{|1\rangle,|2\rangle,|3\rangle\}$, we have the evolution:

$$U_{b1}={\rm e}^{-{\rm i}\omega_1 t_1}\Lambda_1\,{\rm i}U_1, \tag{13}$$

with $\Lambda_1={\rm diag}({\rm e}^{{\rm i}a_1},{\rm e}^{{\rm i}a_2},{\rm e}^{{\rm i}a_3})$ and $a_1=-3(|\Omega_1|^2+|\Omega_2|^2)t_1/(2\Delta)-\pi/2$, $a_2=-\omega_1 t_1$, $a_3=-\omega_2 t_1$. The realization of the U_2-evolution is relatively simple, as it is only required to drive the transition $|1\rangle\leftrightarrow|2\rangle$ under the Hamiltonian Eq. (6) with $\Omega_2=0,\Delta=0$. In the interaction picture, this Hamiltonian reads $H_2=\Omega_1|1\rangle\langle 2|+\Omega_1^*|2\rangle\langle 1|+\omega_{31}|3\rangle\langle 3|$, which delivers an evolution $U_{b2}={\rm e}^{-{\rm i}\nu_1 t_2|1\rangle\langle 1|}\widetilde{U}_2$ with

$$\widetilde{U}_2=\frac{1}{\sqrt{3}}\begin{pmatrix}-\sqrt{2}\,{\rm i}\,{\rm e}^{-{\rm i}\theta_2} & 0\\ {\rm i}\,{\rm e}^{{\rm i}\theta_2} & -\sqrt{2} & 0\\ 0 & 0 & \sqrt{3}{\rm e}^{{\rm i}\omega_{31}t_2}\end{pmatrix},\quad \theta_2=\frac{\Omega_1}{|\Omega_1|}, \tag{14}$$

in Schrödinger picture for $\sin(\Omega t_2)=-1/\sqrt{3}$. It is easily to prove

$$U_{b2}({\rm i}\Lambda_1)=({\rm i}\Lambda_2)U_2, \tag{15}$$

where $\Lambda_2={\rm diag}({\rm e}^{{\rm i}b_1},{\rm e}^{{\rm i}b_2},{\rm e}^{{\rm i}b_3})$, and $b_1=a_1$, $b_2=a_2-\nu_1 t_2$, $b_3=a_3+\beta_2 t_2$ for $\theta_2+a_1-a_2=-\pi/6$. Thus, after these operations, the evolution $({\rm i}\Lambda_2)U_2U_1$ is implemented.

Continuously, by applying a resonant pulse with the frequency $\nu_2 = \omega_{31}$ and the relevant duration satisfying the condition $\sin(|\Omega_2|t) = 1/\sqrt{2}$, the evolution

$$\widetilde{U}_3 = \frac{1}{\sqrt{2}} \begin{pmatrix} 1 & 0 & -\mathrm{i}\,\mathrm{e}^{-\mathrm{i}\theta_3} \\ 0 & -\mathrm{i}\,\mathrm{e}^{-\mathrm{i}(\omega_{21}-\Delta/2)t_2} & 0 \\ \mathrm{e}^{-\mathrm{i}\theta_3} & 0 & 1 \end{pmatrix} \tag{16}$$

could be implemented. Note that $\widetilde{U}_3(\mathrm{i}\Lambda_2) = \mathrm{i}\Lambda_3 U_3$, with $\Lambda_3 = \mathrm{diag}(\mathrm{e}^{\mathrm{i}c_1}, \mathrm{e}^{\mathrm{i}c_2}, \mathrm{e}^{\mathrm{i}c_3})$, $c_1 = b_1$, $c_2 = b_2 - (\omega_{21} - \Delta/2)t_3$, $c_3 = b_3 - \nu_2 t_2$. This means that, after the above three-step operation, we have realized the evolution $\mathrm{i}\Lambda_3 U_3 U_2 U_1$. The last step is required to realize the evolution $U_4(\mathrm{i}\Lambda_3) = \mathrm{i}U_D$, i.e., $U_4 = U_D\Lambda_3^{-1}$. As $U_D\Lambda_3^{-1}$ is just a diagonal matrix with three independent phase parameters, the evolution U_4 can be achieved by only a free evolution with duration t_4, followed by a driving with duration t_5 which is largely detuning from the transition $|1\rangle \leftrightarrow |2\rangle$, and a global phase $\mathrm{e}^{\mathrm{i}x}$. This largely detuning driving leads to an evolution under the effective Hamiltonian $H_5 = -(|\Omega_1|^2/\Delta)|1\rangle\langle 1| + (\omega_{21} + |\Omega_1|^2/\Delta)|2\rangle\langle 2| + \omega_{31}|3\rangle\langle 3|$. If the parameters t_4, t_5, x delivered in these evolution processes are properly set as

$$\begin{aligned} t_4 &= \frac{\lambda}{\omega_{31}} - \frac{\chi}{\zeta|\Omega_1|^2}\left(\Delta + \frac{|\Omega_1|^2}{\omega_{31}}\right), \\ t_5 &= \frac{\chi\Delta}{\zeta|\Omega_1|^2}, \\ x &= -\frac{\Delta}{|\Omega|^2}\left(c_1 + \frac{\pi}{2}\right) - \frac{\chi}{\zeta}, \end{aligned} \tag{17}$$

where $\lambda = c_{31} - 5\pi/6$, $\chi = -c_{21} + 4\pi/6 - \omega_{21}\lambda/\omega_{31}$ and $\zeta = \omega_{21}/\omega_{31} - 2$ with $c_{j1} = c_j - c_1$ $(j = 2, 3)$, we have

$$U_D\Lambda_3^{-1} = \mathrm{e}^{\mathrm{i}x} U_5 U_6 \tag{18}$$

with

$$\begin{aligned} U_5 &= \mathrm{diag}(1,\ \mathrm{e}^{-\mathrm{i}\omega_{21}t_4},\ \mathrm{e}^{-\mathrm{i}\omega_{31}t_4}), \\ U_6 &= \mathrm{diag}(\mathrm{e}^{\mathrm{i}|\Omega_1|^2 t_5/\Delta},\ \mathrm{e}^{-\mathrm{i}(\omega_{21}+|\Omega_1|^2/\Delta)t_5},\ \mathrm{e}^{-\mathrm{i}\omega_{31}t_5}). \end{aligned}$$

Therefore, with the evolutions demonstrated above the required QFT operation $U_{\mathrm{QFT}}^{(3)}$ can be implemented.

Similarly, the inverse of the QFT can be implemented in the similar way by performing the $U_1^\dagger \to U_D^\dagger$ in the reverse order as $U_{\mathrm{QFT}}^{3\dagger} = U_1^\dagger U_2^\dagger U_3^\dagger U_D^\dagger$. Note that, after realization of the $U_1^\dagger$, there will be an extra phase shift $\mathrm{e}^{\mathrm{i}\Lambda}$ while obtaining $U_{\mathrm{QFT}}^{3\dagger}$, where Λ denotes a real diagonal matrix. This extra phase shift can be removed by applying some extra operations. However actually there is no need to remove it, because it only introduces a phase on each state $|1,2,3\rangle$, which will not affect the final population measurement. Furthermore, actually, there is also no need to implement the diagonal matrix U_D in U_{QFT}^3 and $U_{\mathrm{QFT}}^{3\dagger}$. The reason is that, without U_D, the final output state can be theoretically expressed as $U_{\mathrm{QFT}}^{3\dagger} U_D P(\theta) U_D^\dagger U_{\mathrm{QFT}}^3 = U_{\mathrm{QFT}}^{3\dagger} P(\theta) U_{\mathrm{QFT}}^3$ since U_D commutes with $P(\theta)$.

Here, after the phase shift the state is $|\psi_2(\theta)\rangle = \frac{1}{\sqrt{3}}(|1\rangle + \mathrm{e}^{-\mathrm{i}(\omega_2 T+\theta)}|2\rangle + \mathrm{e}^{-\mathrm{i}(\omega_3 T-\theta)}|3\rangle$, where $\theta = \delta T$ (with $\delta = g\mu_{\mathrm{B}}\Delta B/\hbar$) denotes the phase to be estimated and T the free evolution time. By choosing a specific T and the frequencies ω_2 and ω_3, which can be realized by applying an external magnetic field, we have $\omega_2 T = 2n\pi$ and $\omega_3 T = 2m\pi$ with n, m being integers. Then state $|\psi_2(\theta)\rangle$ becomes $|\psi_2(\theta)\rangle = \frac{1}{\sqrt{3}}(|1\rangle + \mathrm{e}^{-\mathrm{i}\theta}|2\rangle + \mathrm{e}^{\mathrm{i}\theta}|3\rangle$. Note that, if exchange the phases of states $|1\rangle$ and $|2\rangle$, it will turn to the standard model. However, there is no need to do that, since the populations measurement after the inverse QFT are almost the same only diver in the order of populations of states $|2\rangle$ and $|3\rangle$. Figure 6 shows the results of populations of states $|1,2,3\rangle$, denoted by $P_{1,2,3}$, respectively. We can see that P_1, P_3 and P_2 differ from each other only by an amount of translation of $2\pi/3$, which is the same as the standard model (not shown in the figure) with $P_2 \leftrightarrow P_3$.

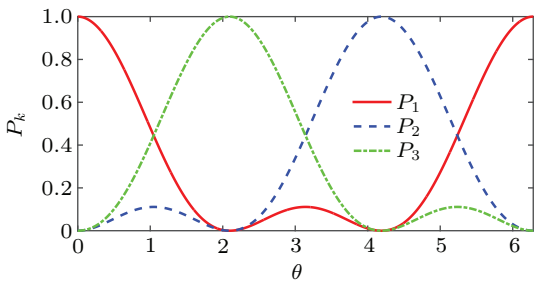


Fig. 6. The populations of states $|1\rangle$, $|2\rangle$ and $|3\rangle$ as a function of phase θ.

After the inverse QFT, the output atomic state of the three-level IFR can be expressed as

$$|\psi_3(\theta)\rangle = \frac{1}{3}[1 + \mathrm{e}^{-\mathrm{i}\theta} + \mathrm{e}^{\mathrm{i}\theta}]|1\rangle + |\varphi\rangle^\perp, \tag{19}$$

with $\langle 1|\varphi\rangle^\perp = 0$. Then the population of the ground state $|1\rangle$ can be calculated with

$$\langle \hat{P}_1(\theta)\rangle = \frac{1}{9}(1 + 2\cos\theta)^2, \tag{20}$$

and $P_2(\theta) = P_1(\theta + 2\pi/3)$, $P_3(\theta) = P_1(\theta - 2\pi/3)$, which are shown in Fig. 6. Using the error-propagation formula, we can derive the measurement uncertainty of a single projective measurement as well as the ultimate bound of the projective measurements, characterized with the correspondent Fisher information, which is defined as $F(\theta) = \sum_{k=1,2,3} |\partial_\theta P_k(\theta)|^2/P_k$. Figure 7 shows the sensitivities of single projective measurements P_k and the corresponding Fisher information. From Fig. 7 we can see that: (i) Each single projective measurement has its own optimal parameter regime that approaches the ultimate bound of QFI, for example, when $\theta \ll 1$, measurement P_1 can reach this bound, which is an optimal measurement. (ii)

From the point of FI, the projective measurements on all states is an optimal POVM whose FI is exactly equal to the QFI, which is also true for any finite multi-level case (not shown in figure).

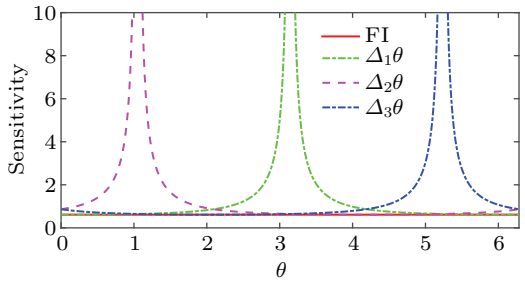


Fig. 7. The sensitivities characterized by the error-propagation formula, $\Delta_k\theta = \sqrt{P_k - P_k^2}\big/|\partial_\theta P_k|$, of population P_k (dashed) and the Fisher information (red solid), $\Delta_F\theta = 1/\sqrt{F(\theta)}$, corresponding to the projective measurements POVM ($P_{1,2,3}$).

With the phase $\theta = \delta T_0$ determined, the detuning δ can be derived such that the magnetic field $\Delta B = \hbar\delta/(g\mu_B)$ can be estimated, with μ_B being the Bohr magneton and g denoting the g-factor. Specifically, for a weak magnetic field required to be estimated, e.g., $B_z \sim \ln T$,[35,37] and for the typical free evolution duration $t \sim 0.3$ ms, Fig. 8 shows clearly that the reachable sensitivity of the IFRs with the present three-level NV-centers really beats the optimal bound in the original atomic IFRs using the usual two-level ones.

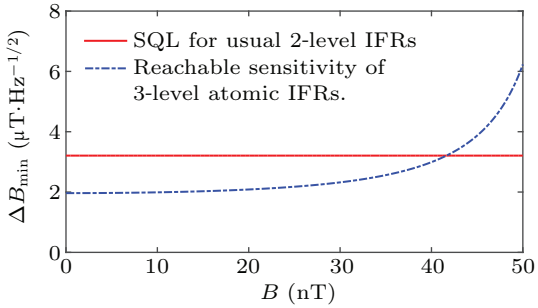


Fig. 8. Reachable sensitivity $\Delta B_{\min}$ vs the measured magnetic field strength B, implemented by the IFRs with single two-levels NV centers (red solid line) which is given as $\Delta B_{\min} = \hbar/(g\mu_B\sqrt{T_2 T})$ with T and T_2 denoting the measurement and coherent time, respectively,[37] and three-level (blue dash-dot line) NV centers, respectively. Here, the free evolution time T_0 is typically set as $\pi/10$ ms.[35] It is seen that reachable sensitivity with the three-level atomic IFRs is higher than that with the usual two-level atomic IFRs for the applied weak magnetic field, i.e., $B < 40$ nT.

Note that, the sensitivity of the above phase estimation can also be enhanced by performing the IFRs with only two spin basis $\{-1,+1\}$ (states $|2\rangle,|3\rangle$) for phase integration, which is called the double quantum (DQ) coherence magnetometry (Refs. [39,40]), since it accumulates phase at twice the rate of traditional single quantum (SQ) coherence magnetometry with states $|1\rangle$ and $|2\rangle$ (or $|3\rangle$). Though DQ magnetometry provides enhanced susceptibility to target magnetic-field signals while also making the spin coherence as twice as being sensitive to magnetic noise, making the spin coherence time for $|2\rangle \leftrightarrow |3\rangle$ is usually shorter than $|1\rangle \leftrightarrow \{|2\rangle,|3\rangle\}$.[41] Many schemes have been put forward to prolong the coherent time by suppressing the dephasing, including the dynamical decoupling and quantum teleportation.[41–43]

4. Discussion and conclusion

Probably, one of the most challenges to experimentally demonstrates the proposed multilevel atomic IFRs such that the implementations of the required QFTs are relatively complicated and their fidelities are certainly limited by various operational imperfections (due to the inevitable noises). This is one of the common obstacles for the current implementations of all the desired quantum coherence manipulations. In this work, we have shown how to implement a QFT with pulse sequence in a V-type three-level atom with the known energy splittings. In practical cases, the external field (to be estimated) may exist during the whole process and can always not be turned off before and after the phase integration, and thus the implementations of the QFT may be imperfect. Specifically, we suppose that the real frequency of states $|2\rangle$ and $|3\rangle$ is symmetrically shift by a relative small detuning δ as $\omega_2 - \delta$ and $\omega_3 + \delta$, due to the Zeeman effect of a external magnetic field. Under this assumption, the Hamiltonians for implementing the evolution U_1 to U_D should be modified. Firstly, the Hamiltonian $\widetilde{H_1}$ in Eq. (11) would be changed to

$$\begin{aligned} H_e = \frac{1}{2(\Delta^2-\delta^2)}\Big\{ & -3\big[\Delta(|\Omega_1|^2+|\Omega_2|^2) \\ & +\delta(|\Omega_2|^2-|\Omega_1|^2)\big]|1\rangle\langle 1| \\ & +\big[\delta(|\Omega_1|^2+|\Omega_2|^2)+\Delta(|\Omega_2|^2-|\Omega_1|^2)\big] \\ & \times\big(|2\rangle\langle 2|-|3\rangle\langle 3|\big)\big(2\Delta\Omega_1\Omega_2^*|2\rangle\langle 3|+\text{H.c.}\big)\Big\}. \end{aligned} \quad (21)$$

Under the condition $\Delta \gg \delta$, neglecting the terms δ/Δ, Hamiltonian H_e is the same as $\widetilde{H}_1$ with $\Delta_1 = \Delta_2 = \Delta$. Considering the first term of the Magnus expansion, we have

$$\begin{aligned} \mathscr{R}_1 = & \ \mathrm{i}\int_0^{t_1} H(t)\,\mathrm{d}t = \frac{\Omega_1^*}{\Delta_1}(\mathrm{e}^{\mathrm{i}\Delta_1 t}-1)|1\rangle\langle 2| \\ & +\frac{\Omega_2^*}{\Delta_2}(\mathrm{e}^{\mathrm{i}\Delta_2 t}-1)|1\rangle\langle 3|+\text{H.c.} \end{aligned} \quad (22)$$

In the case of $\delta = 0$ this term $\mathscr{R}_1 \approx 0$ can be neglected by choosing $\Omega_{1,2} \ll \Delta$ and $\Delta t_1 \approx 2n\pi$. As $\delta \neq 0$, due to $\left|\frac{\Omega_{1(2)}^*}{\Delta_{1(2)}}(\mathrm{e}^{\mathrm{i}\Delta_{1(2)}t}-1)\right| \sim \frac{\delta}{|\Omega_{1(2)}|}$, we find that $\mathscr{R}_1$ is in the order of $\delta/|\Omega| \ll 1$ and thus can be safely neglected. In the realistic case of NV center, the frequency of $\omega_{2,3}$ is in the order of GHz, and the small frequency shift caused by a supposed small magnetic field of nT scale is just in the order of kHz. Therefore, the small detuning δ has little effect on the realization of evolution U_1. Secondly, the Hamiltonian H_2 under detuning becomes

$$H_{2d} = \Omega_1|1\rangle\langle 2| + \Omega_1^*|2\rangle\langle 1| - \delta|2\rangle\langle 2| + (\omega_{31}+\delta)|3\rangle\langle 3|. \quad (23)$$

The corresponding evolution is

$$U_{2d} = \left[\cos(\Omega_1' t_2)I - \mathrm{i}\sin(\Omega_1' t_2)\boldsymbol{n}\cdot\boldsymbol{\sigma}\right] \times \exp\left[\mathrm{i}(\omega_{31}+3\delta/2)t_2|3\rangle\langle 3|\right],$$

with $\Omega_1' = \sqrt{\Omega_1^2+\delta^2/4}$. Here, I and $\boldsymbol{\sigma}$ are the identity and Pauli operators of two-level states $|1\rangle$ and $|2\rangle$, and $\boldsymbol{n} = (|\Omega_1|\cos(\theta_2), |\Omega_1|\sin(\theta_2), \delta/2)/\Omega_1'$. Consequently, under the condition $\Omega_1 \gg \delta$, the evolution of H_{2d} can be approximatively obtained as

$$U_{2d} \approx \widetilde{U}_2 + \mathrm{diag}\left(\left[\frac{\mathrm{i}\delta}{2\sqrt{3}\Omega_1}, \frac{-\mathrm{i}\delta}{2\sqrt{3}\Omega_1}, \mathrm{e}^{\frac{\mathrm{i}3\delta t_2}{2}}\right]\right), \quad (24)$$

with the same pulse time $t_2 \sim \Omega_1^{-1}$. Similarly, by adding a detuning δ to Hamiltonians H_3, H_4 and H_5, the corresponding unperfect evolution of U_3, U_4, U_5 can also be designed. Finally, the imperfect QFT U_{QFT}^d with the detuning δ can be constructed.

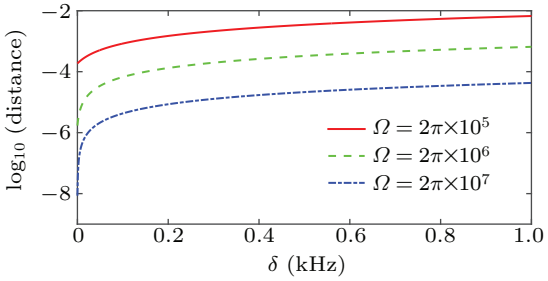


Fig. 9. The dependence of population of state $|1\rangle$ on detuning δ with different Rabi-frequency Ω. The distance is defined as $\max_{kl}\{|(U_{\mathrm{QFT}}^d - U_{\mathrm{QFT}}^3)_{kl}|/|(U_{\mathrm{QFT}}^3)_{kl}|\}$, where U_{QFT}^3 and U_{QFT}^d denote the perfect and the imperfect QFT with the detuning δ. The frequencies of states $|1,2,3\rangle$ are supposed as $\omega_1 = 0$, $\omega_2 = 0.96$ GHz, $\omega_3 = 1.92$ GHz.

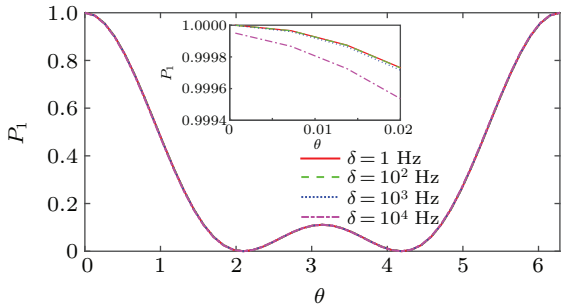


Fig. 10. The measurement population of state $|1\rangle$ as a function of phase θ under different detuning δ. Here Rabi frequencies are all set as $2\pi\times 10^6$ with the large detuning $\Delta = 0.1$ GHz.

Figure 9 shows the dependence of the distance between the theoretical imperfect QFT matrix U_{QFT}^d and the true QFT matrix U_{QFT}^3 with and without the detuning δ. The distance is defined as the maximum absolute value of the matrix elements $|(U_{\mathrm{QFT}}^d - U_{\mathrm{QFT}}^3)_{kl}|/|U_{\mathrm{QFT}}^3)_{kl}|$. It is seen that the distance depends not only on the detuning δ but also on the Rabi frequency Ω. If δ is significantly small, a small error in the order of δ/Ω exists. To further check the validity of the QFT with the detuning, we also plot the dependence of the populations of the ground state $|1\rangle$ on the phase θ for different detunings in Fig. 10. One can see that a very small difference (less than 10^{-3}) occurs, even for $\delta = 10$ kHz. From the above analyses, we can draw a conclusion that the proposed interferometry works even the level-spacing is not known exactly.

In conclusion, via replacing the Hadmard gates by a pair of QFTs we generalize the original Ramsey IFR with a two-level atom to a new IFR with a multilevel atom. The sensitivity of the phase estimations with the proposed M-level IFRs could be enhanced by a factor of $(M^2-1)/3$ compared with the usual two-level cases. Specifically, our generic proposal has been demonstrated with single three-level NV centers in diamond to improve the sensitivity of the magnetometery. Furthermore, considering the practical application, we also investigate the effect of imperfection of the evolutions on the phase estimation sensitivity by considering the impact of a small detuning, caused by an external field, on the realization of QFT. Anyway, given the IFRs proposed here using only single atoms without any inter-atom quantum entanglement and possessing the significant improvement of sensitive bound, its experimental realization and application should be valuable and interesting.

References

[1] Giovannetti V, Lloyd S and Maccone L 2011 *Nat. Photon.* **5** 222
[2] Ramsey N F 1950 *Phys. Rev.* **78** 695
[3] Born M and Wolf E 1999 *Principles of Optics* 7th edn. (New York: Cambridge University Press) pp. 337–338
[4] Pezzé L and Smerzi A 2008 *Phys. Rev. Lett.* **100** 073601
[5] Li H M, Xu X X, Yuan H C and Wang Z 2016 *Chin. Phys. B* **25** 104203
[6] Giovannetti V, Lloyd S and Maccone L 2004 *Science* **306** 1330
[7] Jones J A, Karlen S D, Fitzsimons J, Ardavan A, Benjamin S C, Briggs G A D and Morton J J L 2009 *Science* **324** 1166
[8] Katori H 2011 *Nat. Photon.* **5** 203
[9] Vahlbruch H, Chelkowski S, Hage B, Franzen A, Danzmann K and Schnabel R 2006 *Phys. Rev. Lett.* **97** 011101
[10] Schnabel R, Mavalvala N, McClelland D E and Lam P k 2010 *Nat. Commun.* **1** 121
[11] Abbott B P, *et al.* 2016 *Phys. Rev. Lett.* **116** 241103
[12] Peters A, Chung K Y, Young B, Hensley J and Chu S 1997 *Philos. Trans. R. Soc. London Ser. A* **355** 2223
[13] Angelis M de, Bertoldi A, Cacciapuoti L, Giorgini A, Lamporesi G, Prevedelli M, Saccorotti G, Sorrentino F and Tino G M 2009 *Meas. Sci. Technol.* **20** 22001
[14] Peters A, Chung K Y and Chu S 2001 *Metrologia* **38** 25
[15] Li W D, He T C and Smerzi A 2014 *Phys. Rev. Lett.* **113** 023003
[16] Gustavson T L, Bouyer P and Kasevich M A 1997 *Phys. Rev. Lett.* **78** 2046
[17] Leibfried D, Barrett M D, Schaetz T, Britton J, Chiaverini J, Itano W M, Jost J D, Langer C and Wineland D J 2004 *Science* **304** 1476
[18] D'Ariano G M and Paris M G A 1997 *Phys. Rev. A* **55** 2267
[19] Chwedeńczuk J, Piazza F and Smerzi A 2013 *Phys. Rev. A* **87** 033607
[20] Pezzé L and Smerzi A 2013 *Phys. Rev. Lett.* **110** 163604
[21] Anisimov P M 2010 *Phys. Rev. Lett.* **104** 103602
[22] Gross C 2012 *J. Phys. B* **45** 103001
[23] Hou L L, Sui Y X, Wang S and Xu X F 2019 *Chin. Phys. B* **28** 44203
[24] Huelga S F, Macchiavello C, Pellizzari T, Ekert A K, Plenio M B and Cirac J I 1997 *Phys. Rev. Lett.* **79** 3865
[25] Mitchell M W, Lundeen J S and Steinberg A M 2004 *Nature* **429** 161
[26] Motes K R, Olson J P, Rabeaux E J, Dowling J P, Olson S J and Rohde P P 2015 *Phys. Rev. Lett.* **114** 170802
[27] Olson J P, Motes K R, Birchall P M, Studer N M, LaBorde M, Moulder T and Dowling J P 2017 *Phys. Rev. A* **96** 013810
[28] Dhand I, Khalid A, Lu H and Sanders B C 2016 *J. Opt.* **18** 035204

[29] Cotter J P and Cameron R P 2019 *J. Phys. Commun.* **3** 045012

[30] Crespi A, Osellame R, Ramponi R, Brod D J, Galv an E F, Spagnolo N, Vitelli C, Maiorino E, Mataloni P and Sciarrino F 2013 *Nat. Photon.* **7** 545

[31] Weitz M, Heupel T and Hänsch T W 1996 *Phys. Rev. Lett.* **77** 2356

[32] Zhuang M, Huang J and Lee C 2018 *Phys. Rev. A* **98** 033603

[33] Petrovic J, Herrera I, Lombardi P, Schäfer F and Cataliotti F S 2013 *New J. Phys.* **15** 043002

[34] Braunstein S L and Caves C M 1994 *Phys. Rev. Lett.* **72** 3439

[35] Rondin L, Tetienne J P, Hingant T, Roch J F, Maletinsky P and Jacques V 2014 *Rep. Prog. Phys.* **77** 056503

[36] Wang P, Yuan Z, Huang P, Rong X, Wang M, Xu X and Du J 2015 *Nat. Commun.* **6** 6631

[37] Maze J R, Stanwix P L, Hodges J S, Hong S, Taylor J M, Cappellaro P, Jiang L, Gurudev Dutt M V, Togan E, Zibrov A S, Yacoby A, Walsworth R L and Lukin M D 2008 *Nature* **455** 644

[38] Klimov A B, Guzmãn R, Retamal J C and Saavedra C 2003 *Phys. Rev. A* **67** 062313

[39] Fang K, Acosta V M, Santori C, Huang Z, Itoh K M, Watanabe H, Shikata S and Beausoleil R G 2013 *Phys. Rev. Lett.* **110** 130802

[40] Mamin H J, Sherwood M H, Kim M, Rettner C T, Ohno K, Awschalom D D and Rugar D 2014 *Phys. Rev. Lett.* **113** 030803

[41] Bauch E, Hart C A, Schloss J M, Turner M J, Barry J F, Kehayias P, Singh S and Walsworth R L 2018 *Phys. Rev. X* **8** 031025

[42] Shin C S, Avalos C E, Butler M C, Wang H J, Seltzer S J, Liu R B, Pines A and Bajaj V S 2013 *Phys. Rev. B* **88** 161412

[43] Matsuzaki Y, Benjamin S, Nakayama S, Saito S and Munro W J 2018 *Phys. Rev. Lett.* **120** 140501